Directly Emitting a High-Power Phase-Locked Laser Array by an Internal Phase Sensing System

Jinhu Long, Shuyue He, Qi Chang, Zhiqiang Gao, Yanxing Ma, Rongtao Su, Pengfei Ma, and Pu Zhou

***Abstract*—In this article, we experimentally presented a compact, packaged high-power coherent fiber laser array based on an internal phase sensing technique. In the experiment, a laser array with three beamlets was utilized for experimental presentation. The power output of each laser channel was increased to exceed 500 W. Owing to the exceptional system design and effective thermal management, the internal phase sensing system maintained a remarkable level of performance. When the dynamic phase noise was compensated effectively by the stochastic parallel gradient descent (SPGD) algorithm, the high-power laser array was combined with phase-locked synchronization and directly emitted to the free space. When the output combined power was increased from 3 W to 1.5 kW, the phase deviation remained to be less than λ/27. In addition, the phase control error, element expansion, and further power scaling were fully discussed. This work may offer a practical reference for designing the compact, high-power fiber laser array.**

***Index Terms*—Fiber laser, laser array, coherent beam combining, phase control, internal phase sensing.**

I. Introduction

OWING to its high efficiency and excellent beam quality, the high-power fiber laser is demanded in various applications, such as industrial processing and scientific research [1], [2], [3]. In the past decades, extensive research has been investigated to develop the high-power fiber laser, the output power has been scaled to be dozens of kW [4], [5], [6], [7], [8]. Nevertheless, the further power scaling of a monolithic fiber laser remains a critical challenge due to the nonlinear effects, transverse mode instability [9], [10], [11], and so on. As a practical technique for obtaining a high-power laser, the coherent beam combining (CBC) technique can scale the output power while maintaining excellent beam quality [12], [13], [14]. Nowadays, the number of combined elements has been expanded to be 100 levels [15], [16], [17], [18], and the output power has also been scaled to be over 10 kW [19], [20], [21]. However, further power scaling and element expansion face challenges.

Generally, phase locking is the key to a CBC system, which needs to detect the feedback optical signal of the output laser to actively lock the phase. In practical implementation, the laser array is firstly combined and expanded to obtain a high fill factor [22], [23]. Then, a beam splitter is usually set in the optical path to sample the expanded laser array after they are emitted to the free space, namely the external phase sensing technique [24], [25], [26]. At last, some mature phase-locking techniques are applied to lock the phase, such as the dithering technique [27], [28], [29], the stochastic parallel gradient descent (SPGD) algorithm [30], [31], [32], interference measurement [18], [33], [34], and machine learning [35], [36], [37], [38], [39], etc. Despite that the external phase sensing technique has exhibited impressive performances for phase locking, further power scaling still faces challenges. The emitted laser array will have a large cross section as increasing the combined elements, requiring large aperture optical devices to detect the optical signal. For one thing, these devices would cause inconvenience, the CBC system will be bulk [25], [40]. For another thing, long free-space propagation is required to achieve beam reduction for fitting the small aperture phase sensor [40], which would raise the practical difficulties for phase locking. These problems prevent the CBC systems from moving towards practical application. Fortunately, an internal sensing technique has been put forward and utilized [24], [26], [41]. In contrast to the external sensing technique, this technique can lock the phase by the all-fiber architecture. Nonetheless, the power scaling capacity is limited by the asymmetric fiber couplers. Addressing the problem, in the previous work, we proposed and experimentally demonstrated a compact internal sensing technique, one can lock the phase before forming a large cross-section laser array [25]. The power scaling capacity, however, has not yet been experimentally demonstrated due to certain challenges. On the one hand, the thermal effects in the high-power CBC system can impact its performance and pose practical difficulty in system design. On the other hand, broadening of the laser seed's spectral linewidth is necessary to suppress stimulated Brillouin scattering (SBS) effect [23], but this unavoidably reduces laser coherence length and subsequently diminishes CBC efficiency. This presents a challenge in achieving phase locking. Therefore, the urgent necessity lies in addressing these challenges and experimentally showcasing the capacity for power scaling.

In this article, a compact, packaged high-power CBC system was presented based on an internal phase sensing technique. We

Manuscript received 18 December 2023; revised 23 December 2023; accepted 5 January 2024. Date of publication 9 January 2024; date of current version 26 January 2024. This work was supported in part by the National Natural Science Foundation of China under Grants 62275272 and 62075242, in part by the Training Program for Excellent Young Innovators of Changsha under Grant kq2206003, and in part by the Postgraduate Scientific Research Innovation Project of Hunan Province under Grant QL20220013. *(Corresponding authors: Rongtao Su; Pu Zhou.)*

The authors are with the College of Advanced Interdisciplinary Studies, National University of Defense Technology, Changsha 410073, China (e-mail: ljh65923@163.com; 839788165@qq.com; changqi14@nudt.edu.cn; 1785719531@qq.com; xm_wisdom@163.com; surongtao@126.com; shandapengfei@126.com; zhoupu203@163.com).

Digital Object Identifier 10.1109/JPHOT.2024.3351734

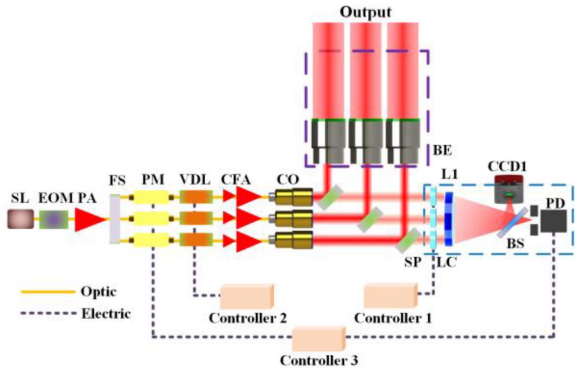

Fig. 1. Experimental setup of the compact laser system based on the internal phase sensing technique. (SL: seed laser; EOM: electro-optic modulator; PA: pre-amplifier; FS: fiber splitter; PM: phase modulator; VDL: variable delay line; CFA: polarization-maintained cascaded fiber amplifier; CO: collimator; SP: small beam splitter; BE: beam expander; LC: liquid crystal; L: lens; BS: beam splitter; CCD: charge-coupled device; PD: photodetector.)

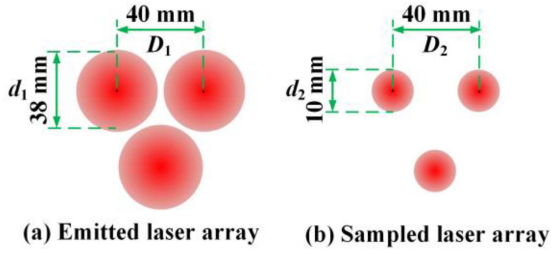

Fig. 2. Schematic drawing of the laser array.

constructed an experimental setup with a three-channel fiber laser array for experimental demonstration. The power output of each laser channel could be increased to exceed 500 W. Owing to the exceptional system design and effective thermal management, the internal phase sensing system maintained a remarkable level of performance. In the experiment, the SPGD algorithm was implemented to lock the dynamic phase noise, the phase deviation was less than $\lambda/27$ when the combined output power was increased from 3 W to 1.5 kW. Consequently, the phase-locked laser array could be directly emitted to the free space. To further enhance the CBC performance, the phase control error, element expansion, and further power scaling capacity were fully discussed and analyzed. The experimental results indicated that our technique would help build a compact, packaged high-power laser array, which could provide a promising solution for obtaining the high-power lasers and their phase control.

II. Experimental Setup

Fig. 1 depicts the experimental configuration, wherein a polarization-maintained single-frequency Yb-doped fiber laser with a central wavelength of 1064 nm serves as the seed laser (SL). The 40 mW laser power from the SL is coupled into an electro-optic modulator (EOM), and the spectral linewidth is broadened to be ~10 GHz based on the phase modulation technique for suppressing the SBS effect [23]. Then, the laser from the EOM is coupled into a pre-amplifier (PA) to scale the power to 400 mW, and then is split into eight channels by a fiber splitter (FS), we choose three-channel lasers for experiment demonstration. Subsequently, each channel laser is coupled into a $LiNbO_3$ phase modulator (PM) and an electric variable delay line (VDL). The PMs have more than 100 MHz modulating bandwidth and operate on 1064 nm, while the VDL could compensate the optical path difference (OPD) with 30 μm. Following that, the output power of each laser channel is scaled to be about 560 W by a polarization-maintained cascaded fiber amplifier (CFA). At last, the laser array from the CFAs is collimated by the collimators (COs). The diameter of each collimated beam is about 10 mm, while the distance between the collimated beams is 40 mm.

To lock the phase and avoid the large optical devices, the feedback signal is detected by the internal phase sensing system, which is circled with a blue dotted line in Fig. 1. The collimated beams are sampled by a splitter (SP) array before they are expanded to the large aperture beams. The reflectivity of SP is 99.9%. The sampled laser transmits through the programmable liquid crystals (LCs) [25], which are used for compensating the phase differences of the emitted laser array. The schematic drawing of the sampled laser array is shown in Fig. 2(b). At last, the sampled laser is focused by a lens (L1). The focused laser is split into two parts by a 50:50 unpolarized beam splitter (BS). One part is truncated by a pinhole with a diameter of 100 μm and detected by a photodetector (PD) for phase error detection. The signal from the PD is used as the power in the bucket (PIB) metric. It is sent into the field programmable gate array (FPGA) controller (Controller 3) for extracting the phase error information. Controller 3 can drive the PMs to actively lock the phase. Another part is detected by a charge-coupled device (CCD1) for visually observing the combination of the sampled laser. The CCD1 is positioned at the focal plane of the L1.

As for the emitted laser array, the diameter of each beamlet is expanded to 38 mm with a beam expander (BE). They are arranged in a regular triangle pattern, as shown in Fig. 2(a). The distance between the adjacent beamlets is 40 mm. Thus, the fill factor is calculated to be 95% with 38 mm/40 mm. Following that, the high-power laser array is emitted to the free space by the laser emitted system, which is circled with the purple dotted line.

III. Experiment Results and Discussion

A. Results of Emitting the Phase-Locked Laser Array

In our experiment, Controller 3 operated at a main frequency of 50 MHz and performed the SPGD algorithm with the iteration frequency of 1 MHz. The experiment was carried out in four steps.

Firstly, Controller 2 was turned on to drive the VDL, and the OPD of the laser array was compensated by the VDL according to the [23]. As a result, the intensity signal detected by the PD would be fluctuated to the maximum after optimizing each VDL's position. Secondly, Controller 3 was turned on, and the internal phase noise was detected and locked by the PMs. Thus,

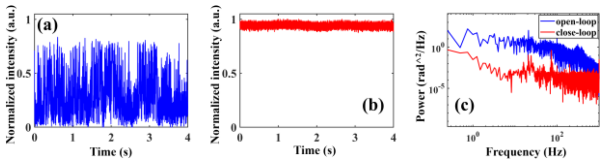

Fig. 3. Normalized time domain signal detected by the PD (a) open loop, (b) close loop, and (c) their power spectral densities.

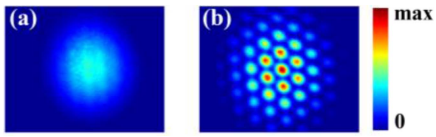

Fig. 4. Irradiance distribution of the sampled laser array detected by the CCD1 when controller 3 was (a) turned off and (b) turned on.

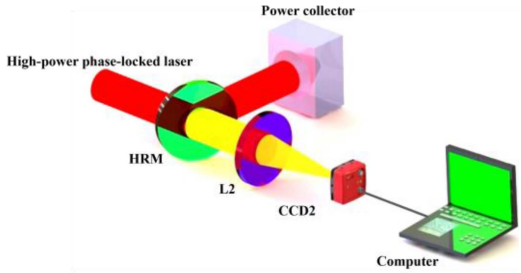

Fig. 5. Schematic drawing of observing the emitted laser array.

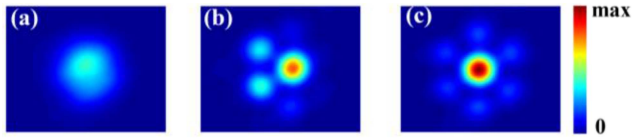

Fig. 6. Irradiance distribution of the emitted laser array detected by the CCD2. (a) Controller 3 and controller 1 were both turned off, (b) controller 3 was turned on while controller 1 was turned off, and (c) controller 3 and controller 1 were both turned on.

the interference fringes of the emitted laser array could be locked stably, and the external phase differences could be measured. Thirdly, the external phase differences among the emitted laser array were measured based on the interference measurement [25]. Then, they were pre-compensated by the LCs, which were droved by Controller 1. Fourthly, the coherent combination of the emitted laser array was observed to present the CBC performance.

The process of phase locking could be observed by the time domain signal that was detected by the PD, as shown in Fig. 3. When Controller 3 was turned off, the time domain signal changed randomly due to environmental noise. The normalized average value was around 0.34, as shown in Fig. 3(a). In contrast, when Controller 3 was turned on and performed the SPGD algorithm continuously, the time domain signal was stably locked to be nearly the maximum. The normalized average value was 0.95, which was 2.8 times when Controller 3 was turned off, as shown in Fig. 3(b). Thus, the phase difference among the sampled laser was locked to be $2n\pi$, where n was an integer. The corresponding residual phase error was calculated to be $\lambda/32$. Furthermore, the power spectral density in the open loop (Controller 3 was turned off) and closed loop (Controller 3 was turned on) was calculated, as shown in Fig. 3(c). We can find that the phase noise of below 900 Hz had been compensated efficiently. In addition, the phase locking speed was calculated to be approximately 2 milliseconds, while the locking range in the experiment was estimated to be around 1 kHz.

Fig. 4 shows the intensity distribution in the far field of the sampled laser array during the phase-locking process. When Controller 3 was turned off, the irradiance distribution of the combined beam had low contrast, and the brightness was weak, as shown in Fig. 4(a). However, when Controller 3 was turned on, the phase difference of the sampled laser array was compensated to be zero by the PMs. As a result, the irradiance distribution was locked stably as shown in Fig. 4(b). The visibility of the interference pattern in the far field was ∼94%.

The above experimental results demonstrated the effective phase locking. To evaluate the CBC efficiency, it is necessary to detect the emitted laser array. In the experiment, a high reflection mirror (HRM) is set in the optical path to extract the high-power emitted laser array, as shown in Fig. 5.

The reflectivity of the HRM is 99.9%. The reflected part is directly emitted to the power collector for power collecting, the total combined power was measured to be ∼3 W. The transmitted part is focused by another lens (L2) to form a far field, which has a long focus length of 2 m. Then, the combined beam in the far field is observed by another CCD2.

Fig. 6 shows the intensity distribution of the emitted laser array during the phase-locking process. When Controller 3 and Controller 1 were both turned off, the phase of each emitted beamlet changed randomly due to the phase noise. The irradiance distribution of the combined beam had low contrast, and the brightness was weak as well, as shown in Fig. 6(a). In comparison, when Controller 3 was turned on while Controller 1 was still turned off, the phase noise could be compensated by the PMs. Therefore, the irradiance distribution of the combined beam was locked stably as shown in Fig. 6(b). However, the irradiance distribution was anomalistic due to the static phase differences among the emitted laser array. Finally, Controller 3 and Controller 1 were both turned on, and the phase differences of emitted laser array were compensated to be zero. As a result, the irradiance distribution was promoted effectively with a prominent central lobe, as shown in Fig. 6(c). To give the CBC efficiency, we calculated the power in the bucket (PIB) ration of the emitted laser array, which served as a representative measure of CBC efficiency. Based on our calculations from Fig. 6(c), we determined that the PIB ratio was approximately 52.7%. Consequently, the achieved CBC efficiency was also measured at 52.7%, slightly below the ideal theoretical calculation of 55%. This indicated that there was a minor loss in CBC efficiency during experimentation, it could be attributed to factors such as pitch and pointing errors, along with other potential perturbations like mechanical effects.

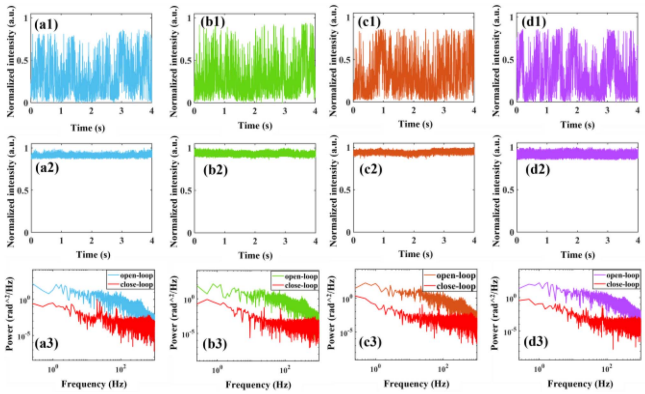

Fig. 7. Normalized time domain signals detected by the PD with different output power (a) 150 W, (b) 300 W, (c) 750 W, and (d) 1.5 kW. (a1)–(d1) open loop, (a2)–(d2) close loop, and (a3)–(d3) their power spectral densities.

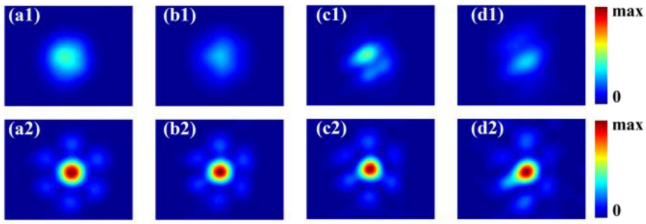

Fig. 8. The irradiance distributions of the emitted laser array detected by the CCD2 with different output power (a) 150 W, (b) 300 W, (c) 750 W, (d) 1.5 kW. (a1)–(d1) Controller 3 and controller 1 were both turned off and (a2)–(d2) controller 3 and controller 1 were both turned on.

B. Results of Emitting the High-Power Phase-Locked Laser Array

To present the power scaling capacity of our system, the combined output power was continuously increased. The output power was measured to be 150 W, 300 W, 750 W, and 1.5 kW, respectively. The time domain signals detected by the PD were shown in Fig. 7. One can find that the internal phase sensing system worked well as increasing the output power, and the time domain signals could be always stably locked to be the maximum, as shown in Fig. 7(a2) to (d2). The normalized average value was 0.92, 0.93, 0.94, and 0.92, respectively. The corresponding residual phase error was calculated to be λ/31, λ/30, λ/31, and λ/27. That meant the CBC system kept a significant performance with a total output power of 1.5 kW. We can also find that the phase noise almost remained unchanged as increasing the power, which was mainly under 900 Hz, as shown in Fig. 7(a3) to (d3). In other words, the total output power can be further scaled. However, we can find that there are several separated peaks in close loop's power spectral densities, the frequency was about 20 Hz, 50 Hz, and 75 Hz, respectively. We deduce the 20 Hz peak was caused by the tilt error, while the other peaks were caused by the power source signal interference. We would optimize our system to avoid these affects in the near future.

The intensity distributions of the emitted laser array were given as well, as shown in Fig. 8. One can see that the intensity distributions all had a prominent central lobe with high fringe contrast and brightness, as shown in Fig. 8(a2) to (d2). The PIB ratios were calculated to be ∼52.3%, ∼52.5%, ∼51.0%, and ∼47%, respectively. Accordingly, the CBC efficiency was ∼52.3%, ∼52.5%, ∼51.0%, and ∼47%, respectively. Owing to the advantages of the internal phase sensing technique, the phase control performance could be kept well when scaling the output power. The combined power of the phase-locked laser array was scaled to 1.5 kW, which may help build a compact and packaged high-power laser.

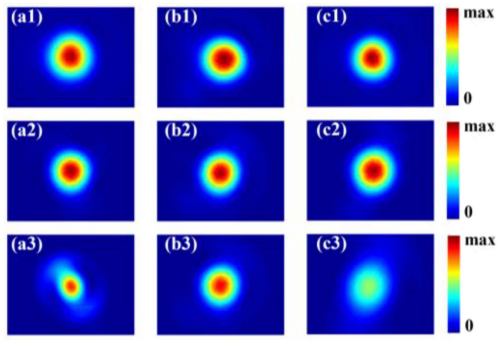

Fig. 9. Irradiance distributions of the laser from different CFAs with different combined output power. (a) The 1st CFA, (b) 2nd CFA, (c) 3rd CFA. (a1)–(c1) 1 W, (a2)–(c2) 750 W, and (a3)–(c3) 1.5 kW.

C. Analysis of the Phase Control Error and Discussion

Here, we presented a high-power phase-locked laser array via the internal phase sensing technique. The combined output power could be scaled from 3 W to 1.5 kW. The above results indicated that the phase control kept a significant performance when increasing the power. However, we should note that the intensity distributions of the combined beams degraded when the power was 1.5 kW, as shown in Fig. 8(d1) and (d2). In this case, the CBC efficiency decreased to 47%. In addition, the corresponding residual phase error also decreased from λ/30 to λ/27. Therefore, to further scale the output power, the phase control error should be analyzed. In the experiment, the water-cool system was optimized to achieve efficient thermal management. In addition, the experiment was carried out in a clean room with a sealed housing, and the surface contamination of optical devices was avoided. Besides, the phase was detected by utilizing several separated beam splitters. The optical devices were heated up by only 4 °C, and the temperature was under 25 °C. Hence, the possible thermal effects of the CBC system could be avoided in a high-power status. We deduce that the phase control error and combined intensity distribution degradation were mainly caused by the beam quality degradation of the CFAs. To verify our deduction, we detected the intensity distribution of the beams from the CFAs, the results were shown in Fig. 9. Fig. 9(a1) to (c1) represent the intensity distributions of the 1st, 2nd, and 3rd beamlets in a 1 W level, respectively. Fig. 9(a2) to (c2) represent the intensity distributions of the 1st, 2nd, and 3rd beamlets when the combined output power was 750 W, while Fig. 9(a3) to (c3) represent the intensity distributions when the combined output

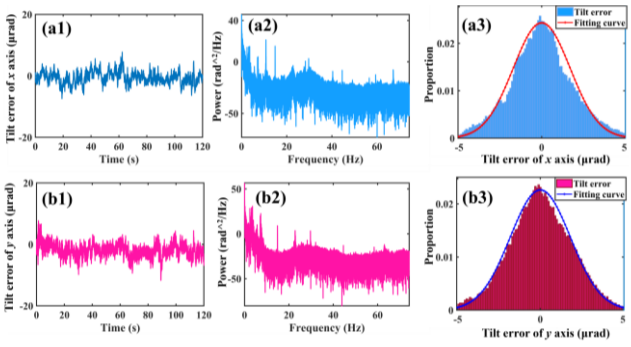

Fig. 10. Results of analyzing the tilt errors. In the x axis direction (a1) the tilt errors, (a2) the spectra analyses, and (a3) the frequency histogram and its fitting curve; In the y axis direction (b1) the tilt errors, (b2) the spectra analyses, and (b3) the frequency histogram and its fitting curve.

power was 1501 W. We can find that the intensity distributions of the 1st, and 3rd beamlets degraded after the power was over 500 W, as shown in Fig. 9(a3) and (c3). The peak power decreased to 0.86, and 0.6 times that of Fig. 9(a2) and (c2), which influenced the phase control.

Meanwhile, the COs were fixed in the optical platform, which could be influenced by the dynamic environmental vibration and the water-cooling system, resulting in beam pointing error and influencing the phase control. Hence, to measure accurately the tilt error, we open only one laser channel, and a high-speed camera was placed at the focal plane of the L1 to record the changing of the focal spot. The high-speed camera worked at 1000 fps and recorded the intensity data with a time of about 12 s. Then, one can get the tilt error from the two-dimensional pattern data according to the reference [18]. The detailed results are shown in Fig. 10. The tilt errors of the x axis and y axis are shown in Fig. 10(a1) and (b1), respectively. The y axis was defined as the direction of gravity. One can find that the tilt error rules were almost the same as each other. However, the maximum of the tilt errors in x axis was 8 μrad, while that was 12 μrad in y axis. The average tilt errors were 1.5 μrad and 2.3 μrad, respectively. We can find that the tilt errors in y axis were larger than that in x axis. The reason was that the mechanical vibration was usually induced in the y axis. Then, we calculated the corresponding spectra of the tilt errors, as shown in Fig. 10(a2) and (b2). As we can see, the main frequencies were both below 20 Hz, which verifies our deduction about the peaks in Fig. 7. At last, the frequency histograms of the tilt errors and their fitting curves were given as well, as shown in Fig. 10(a3) and (b3). One can see that the tilt errors were both in normal distributions, the mean values were both $\sim$0, while the standard deviations were only 1.9 μrad and 2.0 μrad, respectively.

Subsequently, the CBC efficiency loss was further analyzed according to the above data. We carried out the numerical simulation according to the tilt errors, the calculated CBC efficiency was $\sim$54%, which meant the tilt errors would cause the 2% CBC efficiency loss. That meant there was still a 2% CBC efficiency loss due to other errors. To conclude, the CBC efficiency loss was mainly caused by the beam quality degradation of the CFAs, the tilt errors, and other error, such as polarization inconsistency.

Based on the preliminary experiment, the power scaling capacity of the internal phase sensing technique has been demonstrated. The internal phase sensing CBC system demonstrated remarkable performance enhancement in response to the increased output power. Owing to its exceptional system design and effective thermal effects management, a total 1.5 kW laser array with phase locked could be directly emitted to the free space, providing a promising strategy for developing efficient and packageable high-power laser sources with excellent beam quality. We should note that the reason for not using plane mirrors to reduce the lens aperture size in the sampled laser array is to simplify the system [25]. To further scale the output power, there are two methods available. Firstly, the output power of each laser channel can be enhanced. Nowadays, output power of the polarization-maintained fiber amplifier (CFA) has been scaled to be 5 kW [42], which could be utilized in our system. Secondly, expanding the combined beam elements to achieve higher output power is feasible. Recently, the phase locking of nineteen-channel kW fiber laser amplifiers has been presented in the experiment [21]. Moreover, the phase locking of more than 100 beam elements has been demonstrated as well [15], [16], [18]. Hence, the coherent combination of the 100-channel level kW fiber laser amplifiers is feasible. However, we should note that there are still some challenges. The phase control bandwidth would decrease when increasing the beam number, while the tilt errors could severely decrease the CBC efficiency as well [15]. Thus, one should address the challenges in two steps. For one thing, when combining a laser array with hundreds of elements, the whole laser array should be divided into several sub-arrays, each sub-array is detected and compensate the phase noise independently. In this way, the cascaded internal phase control technique can be applied for locking the phases of the whole laser array and improving the control bandwidth [43]. However, the tilt error can have a significant impact on the long-term locking stability when dealing with a large number of fibers in a 2D array. Based on our previous research [25], it is deduced that the locking stability of this high-power CBC system may be limited to several dozen hours. Therefore, it is crucial to ensure compactness and adhere to strict constraints on pitch and pointing to maintain optimal CBC efficiency. For another thing, some tip/tilt control techniques could be used for decreasing the tip/tilt errors, such as the adaptive fiber-optics collimator (AFOC) or a fast piezo steering mirror (FPSM) [44]. Owing to that the caliber of the laser emitting system can be freely designed, our technique is also helpful for building a large aperture high-power laser array, which is beneficial to a wide of applications, such as laser communications [45], and energy transmission [32].

IV. Conclusion

In summary, we experimentally presented a compact, packaged kW laser source in a CBC architecture based on the internal phase sensing technique. In our experiment, a three-channel fiber laser array was utilized for experimental demonstration. The emitted power of each laser channel could be increased to be over 500 W. Owing to the exceptional system design and effective

thermal effects management, the internal phase sensing CBC system demonstrated remarkable performance enhancement in response to the increased output power. The SPGD algorithm was implemented to lock the dynamic phase noise, the phase deviation was less than $\lambda/27$. The CBC efficiency was $\sim$47% when the combined output power was 1.5 kW. In addition, the phase control error, element expansion, and further power scaling capacity were discussed and analyzed. This work could offer a promising reference for obtaining the high-power laser.

ACKNOWLEDGMENT

The authors thank Jian Wu, Wei Li, Hongxiang Chang, Qi Chen, et al. for their help with the experiment setup.

REFERENCES

[1] C. Jauregui, J. Limpert, and A. Tünnermann, "High-power fibre lasers," *Nature Photon.*, vol. 7, pp. 861–867, 2013.
[2] M. N. Zervas and C. A. Codemard, "High power fiber lasers: A review," *IEEE J. Sel. Topics Quantum Electron.*, vol. 20, no. 5, pp. 219–241, Sep./Oct. 2014.
[3] C. N. Danson et al., "Petawatt and exawatt class lasers worldwide," *High Power Laser Sci. Eng.*, vol. 7, 2019, Art. no. e54.
[4] M. O'Connor, V. Gapontsev, V. Fomin, M. Abramov, and A. Ferin, "Power scaling of SM fiber lasers toward 10 kW," in *Proc. Conf. Lasers Electro-Opt./Int. Quantum Electron. Conf., OSA Tech. Dig.*, 2009, Paper CThA3.
[5] F. Beier et al., "Single mode 4.3 kW output power from a diode-pumped Yb-doped fiber amplifier," *Opt. Exp.*, vol. 25, pp. 14892–14899, 2017.
[6] Y. Wang et al., "8-kW single-stage all-fiber Yb-doped fiber laser with a BPP of 0.50 mm-mrad," *Proc. SPIE*, vol. 11260, pp. 273–278, 2020.
[7] S. Du, T. Qi, D. Li, P. Yan, M. Gong, and Q. Xiao, "10 kW fiber amplifier seeded by random fiber laser with suppression of spectral broadening and SRS," *IEEE Photon. Technol. Lett.*, vol. 34, no. 14, pp. 721–724, Jul. 2022.
[8] L. Huang et al., "Homemade confined-doped fiber for 10 kW level fiber laser output with good beam quality," *High Power Laser Part. Beams*, vol. 34, 2022, Art. no. 111002.
[9] V. Distler, F. Möller, M. Strecker, G. Palma-Vega, T. Walbaum, and T. Schreiber, "Transverse mode instability in a passive fiber induced by stimulated Raman scattering," *Opt. Exp.*, vol. 28, pp. 22819–22828, 2020.
[10] C. Stihler, C. Jauregui, S. E. Kholaif, and J. Limpert, "Intensity noise as a driver for transverse mode instability in fiber amplifiers," *PhotoniX*, vol. 1, no. 1, 2020, Art. no. 8.
[11] S. Ren et al., "Experimental study on the impact of signal bandwidth on the transverse mode instability threshold of fiber amplifiers," *Opt. Exp.*, vol. 30, pp. 7845–7853, 2022.
[12] T. Y. Fan, "Laser beam combining for high-power, high-radiance sources," *IEEE J. Sel. Topics Quantum Electron.*, vol. 11, no. 3, pp. 567–577, May/Jun. 2005.
[13] A. Brignon, *Coherent Laser Beam Combining*. Hoboken, NJ, USA: Wiley, 2013.
[14] P. Zhou et al., "Review of coherent laser beam combining research progress in the past decade," *Chin. J. Lasers*, vol. 48, no. 4, 2021, Art. no. 0401003.
[15] H. Chang et al., "First experimental demonstration of coherent beam combining of more than 100 beams," *Photon. Res.*, vol. 8, no. 12, pp. 1943–1948, 2020.
[16] M. Shpakovych et al., "Experimental phase control of a 100 laser beam array with quasi-reinforcement learning of a neural network in an error reduction loop," *Opt. Exp.*, vol. 29, pp. 12307–12318, 2021.
[17] Q. Du, D. Wang, T. Zhou, D. Li, and R. Wilcox, "81-beam coherent combination using a programmable array generator," *Opt. Exp.*, vol. 29, pp. 5407–5418, 2021.
[18] Q. Chang et al., "Experimental phase stabilization of a 397-channel laser beam array via image processing in dynamic noise environment," *J. Lightw. Technol.*, vol. 40, no. 19, pp. 6542–6547, Oct. 2022.
[19] E. Shekel, Y. Vidne, and B. Urbach, "16 kW single mode CW laser with dynamic beam for material processing," *Proc. SPIE*, vol. 11260, pp. 267–272, 2020.
[20] M. Müller et al., "10.4 kW coherently combined ultrafast fiber laser," *Opt. Lett.*, vol. 45, no. 11, pp. 3083–3086, 2020.
[21] J. Wu et al., "Coherently combined fiber laser with 20 kW high power output," *Infrared Laser Eng.*, vol. 50, no. 9, 2021, Art. no. 20210621.
[22] L. A. Beresnev et al., "Design of a noncooled fiber collimator for compact, high-efficiency fiber laser arrays," *Appl. Opt.*, vol. 56, no. 3, pp. B169–B178, 2017.
[23] P. Ma et al., "7.1 kW coherent beam combining system based on a seven-channel fiber amplifier array," *Opt. Laser Technol.*, vol. 140, 2021, Art. no. 107016.
[24] L. Roberts et al., "High power compatible internally sensed optical phased array," *Opt. Exp.*, vol. 24, no. 12, pp. 13467–13479, 2016.
[25] J. Long et al., "Compact internal sensing phase locking system for coherent combining of fiber laser array," *Opt. Laser Technol.*, vol. 148, 2022, Art. no. 107775.
[26] H. Chang et al., "Distributed active phase-locking of an all-fiber structured laser array by a stochastic parallel gradient descent (SPGD) algorithm," *Opt. Exp.*, vol. 30, pp. 1089–1098, 2022.
[27] Y. Ma et al., "Coherent beam combination of 1.08 kW fiber amplifier array using single frequency dithering technique," *Opt. Lett.*, vol. 36, no. 6, pp. 951–953, 2011.
[28] Z. Huang et al., "Active phase locking of thirty fiber channels using multilevel phase dithering method," *Rev. Sci. Instrum.*, vol. 87, no. 3, 2016, Art. no. 033109.
[29] J. Ballato, A. Flores, T. Ehrehreich, R. Holten, B. Anderson, and I. Dajani, "Multi-kW coherent combining of fiber lasers seeded with pseudo random phase modulated light," *Proc. SPIE*, vol. 9728, pp. 363–368, 2016.
[30] C. X. Yu et al., "Coherent combining of a 4 kW, eight-element fiber amplifier array," *Opt. Lett.*, vol. 36, no. 14, pp. 2686–2688, 2011.
[31] C. Geng, W. Luo, Y. Tan, H. Liu, J. Mu, and X. Li, "Experimental demonstration of using divergence costfunction in SPGD algorithm for coherent beam combining with tip/tilt control," *Opt. Exp.*, vol. 21, no. 21, pp. 25045–25055, 2013.
[32] T. Weyrauch et al., "Deep turbulence effects mitigation with coherent combining of 21 laser beams over 7 km," *Opt. Lett.*, vol. 41, no. 4, pp. 840–843, 2016.
[33] M. Antier et al., "kHz closed loop interferometric technique for coherent fiber beam combining," *IEEE J. Sel. Topics Quantum Electron.*, vol. 20, no. 5, pp. 182–187, Sep./Oct. 2014.
[34] I. Fsaifes et al., "Coherent beam combining of 61 femtosecond fiber amplifiers," *Opt. Exp.*, vol. 28, no. 14, pp. 20152–20161, 2020.
[35] T. Hou et al., "Deep-learning-based phase control method for tiled aperture coherent beam combining systems," *High Power Laser Sci. Eng.*, vol. 7, no. 4, pp. 8–14, 2019.
[36] R. Liu, C. Peng, X. Liang, and R. Li, "Coherent beam combination far-field measuring method based on amplitude modulation and deep learning," *Chin. Opt. Lett.*, vol. 18, no. 4, 2020, Art. no. 041402.
[37] D. Wang, Q. Du, T. Zhou, D. Li, and R. Wilcox, "Stabilization of the 81-channel coherent beam combination using machine learning," *Opt. Exp.*, vol. 29, no. 4, pp. 5694–5709, 2021.
[38] A. Mirigaldi, M. Carbone, and G. Perrone, "Non-uniform adaptive angular spectrum method and its application to neural network assisted coherent beam combining," *Opt. Exp.*, vol. 29, no. 9, pp. 13269–13287, 2021.
[39] M. Jiang et al., "Fiber laser development enabled by machine learning: Review and prospect," *PhotoniX*, vol. 3, no. 1, 2022, Art. no. 16.
[40] A. Boju et al., "Small footprint phase locking system for a large tiled aperture laser array," *Opt. Exp.*, vol. 29, no. 8, pp. 11445–11452, 2021.
[41] Y. Yang, C. Geng, F. Li, G. Huang, and X. Li, "Multi-aperture all-fiber active coherent beam combining for free-space optical communication receivers," *Opt. Exp.*, vol. 25, pp. 27519–27532, 2017.
[42] Y. Wang et al., "5 kW near diffraction limit high extinction ratio narrow linewidth polarization maintaining fiber laser," *High Power Laser Part. Beams*, vol. 34, 2022, Art. no. 112002.
[43] J. Long et al., "System design for coherent combined massive fiber laser array based on cascaded internal phase control," *Appl. Opt.*, vol. 61, pp. 10222–10227, 2022.
[44] F. Li, C. Geng, G. Huang, Y. Yang, and X. Li, "Wavefront sensing based on fiber coupling in adaptive fiber optics collimator array," *Opt. Exp.*, vol. 27, pp. 8943–8957, 2019.
[45] C. Geng et al., "Fiber laser transceiving and wavefront aberration mitigation with adaptive distributed aperture array for free-space optical communications," *Opt. Lett.*, vol. 45, pp. 1906–1909, 2020.